

Neutron displacement damage cross sections for SiC *

Hanchen Huang and Nasr Ghoniem

Mechanical, Aerospace and Nuclear Engineering Department, University of California, Los Angeles, CA 90024-1597, USA

Received 17 July 1992; accepted 8 September 1992

Calculations of neutron displacement damage cross sections for SiC are presented. We use Biersack and Haggmark's empirical formula in constructing the electronic stopping power, which combines Lindhard's model at low PKA energies and Bethe–Bloch's model at high PKA energies. The electronic stopping power for polyatomic materials is computed on the basis of Bragg's Additivity Rule. A continuous form of the inverse power law potential is used for nuclear scattering. Coupled intergro-differential equations for the number of displaced atoms j , caused by PKA i , are then derived. The procedure outlined above gives partial displacement cross sections, displacement cross sections for each specie of the lattice, and for each PKA type. The corresponding damage rates for several fusion and fission neutron spectra are calculated. The stoichiometry of the irradiated material is investigated by finding the ratio of displacements among various atomic species. The role of each specie in displacing atoms is also investigated by calculating the fraction of displacements caused by each PKA type. The study shows that neutron displacement damage rates of SiC in typical magnetic fusion reactor first walls will be ~ 10 – 15 dpa MW⁻¹ m²; in typical lead-protected inertial confinement fusion reactor first walls they will be ~ 15 – 20 dpa MW⁻¹ m². For fission spectra, we find that the neutron displacement damage rate of SiC is ~ 74 dpa per 10^{27} n/m² in FFTF, ~ 39 dpa per 10^{27} n/m² in HFIR, and 25 dpa per 10^{27} n/m² in NRU. Approximately 80% of displacement atoms are shown to be of the carbon-type.

1. Introduction

Early calculations of radiation damage rates in monatomic materials have been made on the basis of simplifying assumptions. Jenkins [1] and Sheely [2] used the Kinchin–Pease model to account for the displacement efficiency and calculated the displacement cross sections for iron. Their work was extended and made complete by Doran [3], who used Lindhard's model in accounting for the displacement efficiency and included inelastic (e.g., $(n, 2n)$ and (n, γ)) nuclear reaction channels. Investigation of displacement rates in polyatomic materials soon followed. In the works of Baroody [4] and Andersen and Sigmund [5], the contributions of the electronic stopping to the energy loss were omitted. Realizing the importance of this mechanism of energy loss, Parkin and Coulter [6] accounted for the electronic stopping by using Lindhard's model and solving coupled intergro-differential equations for

the number of displaced atoms. The investigations were applied to MgO, Al₂O₃ and TaO. Their work was further developed to a computer code by Greenwood [7]. Alberman and Lesueur [8] developed a similar computer code (COMPOSI), on the basis of their own formulation to calculate the displacement damage rates in diatomic materials. However, their formulation is not accurate because they assumed that the energy transferred is fixed after the ion travels a distance in the matrix.

In this paper, we present a calculational method for displacement damage in SiC. First, we construct the electronic stopping power based upon Lindhard's [9,10] and Bethe–Bloch's [11,12] formulations, and use Biersack and Haggmark's empirical bridging formula [13]. Secondly, we extend this formulation to polyatomic materials and use Bragg's Additivity Rule, which was experimentally shown to be reasonably accurate within 10–15% [14]. Thirdly, we formulate coupled intergro-differential equations for the number of displaced atoms. The numerical procedure is an extension of the Runge–Kutta method to coupled differential equations. Following these steps, we calculate the partial

* Work supported by the Office of Fusion Energy, US DOE under grant DE-FG03-91ER54115.

displacement cross sections, the damage rates of each atomic specie, the damage rates caused by each PKA type, the total displacement cross section, and the total displacement damage rates of SiC under irradiation conditions of FFTF, HFIR, NRU [15], PROMETHEUS [16] and ARIES4 [17]. Finally, conclusions are given in section 5, especially the implications of these results to simulation experiments of neutron irradiation in non-fusion facilities.

2. Theory

2.1. Electronic stopping power in polyatomic materials

In the low energy range, Lindhard's theory of electronic stopping for energetic ions is well accepted. Although it is proposed by Ziegler et al. [18] that the electronic stopping power of silicon and carbon may behave as $E^{0.35}$ at very low ion energies, we use the Lindhard formulation. The reasons for this choice are two fold: (1) there is not enough experimental data to give accurate electronic stopping cross sections in the very low energy range, and (2) electronic stopping in this range ($E \leq 500$ eV) doesn't have a large effect in displacement damage calculations. The Lindhard electronic stopping cross section is given by [9,10]

$$S_e = \frac{1}{N_2} \left(\frac{dE}{dx} \right)_e = 8\pi e^2 a_0 \frac{Z_1^{7/6} Z_2 v}{Z v_0}, \quad (1)$$

where $Z^{2/3} = Z_1^{2/3} + Z_2^{2/3}$, $v_0 = 2\pi e^2/h$, and $a_0 = 0.529$ Å. Z_1 and Z_2 are charge numbers of the projectile and the target atoms, respectively, e the charge of an electron, v the velocity of the projectile, N_2 the atom density of the target, and h the Planck constant. This formula is valid for PKA energies $E < 25$ keV/amu [18].

In the case of fusion neutron irradiation of low- Z elements, the PKA energy can be high enough so that Lindhard's formulation does not hold anymore. For PKA energies greater than 200 keV/amu, the Bethe-Bloch electronic stopping power is in good agreement with experiments. The Bethe-Bloch stopping cross section is given by [11,12]

$$S_e = \frac{1}{N_2} \left(\frac{dE}{dx} \right)_e = \frac{2\pi Z_{\text{eff}}^2 Z_2 e^4 (M_1/m_e)}{E} \ln \left(\frac{4E}{(M_1/m_e) \bar{I}} \right), \quad (2)$$

where Z_{eff} is an effective charge of the projectile, given by Bohr [19]. E is the energy of the projectile, M_1 the mass of the projectile, m_e the mass of the electron, N_2

the atomic density of the target, and \bar{I} the ionization energy of the target atom. This stopping formulation is valid for PKA energies $E > 200$ keV/amu.

To cover the entire energy range, we propose to extrapolate the formulation of Bethe-Bloch to low energy by linear extrapolation at the highest stopping energy point. The two stopping powers are then bridged according to Biersack and Haggmark's procedure [13], which is given by

$$S_e^{-1} = (S_e)_{\text{Lindhard}}^{-1} + (S_e)_{\text{Bethe-Bloch}}^{-1}. \quad (3)$$

The theoretical prediction of electronic stopping power based on this equation is compared with the experimental data of electronic stopping power in monatomic materials given by Northcliffe [20], and very good agreement is obtained. Since Bragg's Additivity Rule has been experimentally shown to be accurate within 10–15% [14], we extend the electronic stopping power obtained above to polyatomic materials based on Bragg's Additivity Rule. This is given by

$$S_{e \text{ composite}} = \frac{\sum_i A_i N_i S_{e,i}}{\sum_i A_i N_i}, \quad (4)$$

where A_i and N_i are mass number and atomic density of species i , respectively.

2.2. Interatomic potentials and atomic scattering cross sections

Winterbon [21] compared the accuracy of the atomic scattering cross section based on the inverse power law potential with that based on the Thomas-Fermi potential, and found that they are in fairly good agreement, provided that several power laws are used to cover the entire energy range. Therefore, the inverse power law potential, which is very simple, is used in this paper. In applying the inverse power law potential, the main problem to be solved is matching potentials of different powers. Here, we are concerned with the energy transfer process. Therefore, we match different powers by requiring that the atomic stopping cross section is continuous at each transition point. According to Winterbon [21], we have

$$\sigma(E, T) dT = C_m E^{-m} T^{-1-m} dT, \quad (5)$$

where

$$C_m = \frac{\pi}{2} \lambda_m a^2 \frac{A_1}{A_2} \left(\frac{2Z_1 Z_2 e^2}{a} \right)^{2m}$$

and

$$a = \frac{0.4683}{(Z_1^{2/3} + Z_2^{2/3})^{1/2}}.$$

The value of the power m , and the constant λ_m are given by

$$\begin{aligned} (m, \lambda_m) &= (1/3, 1.309) & \text{for } \epsilon \leq \epsilon_2, \\ &= (1/2, 0.327) & \text{for } \epsilon_2 \leq \epsilon \leq \epsilon_1, \\ &= (1, 0.5) & \text{for } \epsilon_1 \leq \epsilon, \end{aligned}$$

where ϵ is the reduced energy $\epsilon = E/e_0$ while $e_0 = Z_1 Z_2 e^2/a$, (ϵ_1, ϵ_2) are transition energies, and A_1 and A_2 are the mass numbers of the projectile and the target, respectively.

Chou and Ghoniem [22] modified this cross section at extremely low energies. They proposed to match the Born-Mayer potential by using an inverse power potential with $m = 0$ and $\lambda_m = 24$ for $\epsilon < \epsilon_3$. According to the matching procedure mentioned above, Chou and Ghoniem found that the transition energies should be chosen as $(\epsilon_1, \epsilon_2, \epsilon_3) = (2-10, 0.369, 0.0234)$. For SiC, we found that a smoother matching can be obtained if we choose $\epsilon_1 = 15$. Therefore the values, $(\epsilon_1, \epsilon_2, \epsilon_3) = (15, 0.369, 0.0234)$ are used in this paper. We compared the results based on these two different matching procedures and found that they give similar results, except that the new matching gives smoother dependence of the damage cross section on energy.

2.3. Governing equations for the number of displaced atoms, ν_{ij}

Assume that the solid contains atoms of type i and j . If a PKA of type i travels a distance dx , it will eventually result in a number of displacements of atoms of type i (ν_{ii}) and a number of atoms of type j (ν_{ij}). Similarly, a PKA of type j will produce ν_{ji} and ν_{jj} . Conservation of atoms implies that each one of these numbers are separately conserved over all possibilities. That is to say that ν_{ij} is conserved before and after interaction. Therefore, we have the following conservation equation

$$\begin{aligned} \nu_{ij}(E) &= \sum_k \int_0^{A_{ik}E} \left[\Gamma(E - T - E_{jd}/\Lambda_{ij}) \nu_{ij}(E - T) \right. \\ &\quad \left. + \Gamma(T - E_{kd})(\delta_{kj} + \nu_{kj}(T)) \right] N_k \sigma_{ik}(E, T) \\ &\quad \times dx dT + \int_0^T \nu_{ij}(E - T_e) N_e \sigma_{ie}(E, T) dx dT \\ &\quad + \left(1 - \sum_k N_k \sigma_{ik}(E) dx - N_e \sigma_{ie}(E) dx \right) \nu_{ij}(E), \end{aligned} \quad (6)$$

where ν_{ij} is the number of displaced atoms of type j caused by PKA of type i , excluding the PKA itself, $\Gamma(x)$ is the step function, N_i the atomic density of species i , $\sigma_{ij}(E, T)$ the differential atomic scattering cross section of species i and j , $\sigma_{ij}(E)$ the total microscopic atomic scattering cross section between species i and j , Λ_{ij} the energy transfer efficiency between species i and j , and δ_{kj} the Kronecker delta function. The first integral represents the number of displacements ν_{ij} if a PKA (of type i) collides with target atoms in traveling through a short distance dx , the displacements induced by the slowed-down PKA, and the displacements induced by the SKA (secondary knock-on atom). The second integral represents the number of displacements ν_{ij} if the PKA collides with electrons in traveling dx . The last term represents the number of displacements ν_{ij} if nothing happens in traveling the distance dx . The collision cascade model will be discussed in more detail in the next section. The reader is referred to Lindhard's work (e.g. ref. [3]) for further explanation of the derivation of eq. (6).

Approximating $\nu_{ij}(\dot{E} - T_e) = \nu_{ij}(E) - T_e(d\nu_{ij}(E)/dE)$ and performing algebraic manipulations, we obtain the following coupled intergro-differential equation

$$\begin{aligned} S_{ie} \frac{d\nu_{ij}(E)}{dE} &= \sum_k f_k \int_0^{A_{ik}E} \left\{ \left[\Gamma(T - E_{kd})(\delta_{kj} + \nu_{kj}(T)) \right] \right. \\ &\quad \times \sigma_{ik}(E, T) dT \\ &\quad \left. + \left[\Gamma(E - T - E_{jd}/\Lambda_{ij}) \nu_{ij}(E - T) - \nu_{ij}(E) \right] \right. \\ &\quad \left. \times \sigma_{ik}(E, T) dT \right\}, \end{aligned} \quad (7)$$

where $S_{ie}(E)$ is the electronic stopping cross section of specie i , f_k the fraction of atom density of specie i in the composite, E_{jd} the displacement threshold of specie j .

Because there is no resonance in the displacement efficiency and the atomic scattering cross section, there is little doubt that the integration could be done attaining high accuracy by using any simple integration procedure. On the other hand, care must be exercised in solving the coupled integral-differential eq. (7). We extended the Runge-Kutta [23] method to two coupled differential equations, and the numerical extension procedure of Runge-Kutta method to 2 coupled differential equations is given in appendix A.

2.4. Collision cascade model

A PKA (of type i) traveling a short distance in binary ceramics may have several collision channels. The PKA may collide with an atom of specie k (k may represent Si or C) and transfer an amount of energy T to the atom. There will be slowed-down PKAs with energy $(E - T)$ and SKAs with energy T after the collision. Both the slowed-down PKAs and SKA's will continue to displace lattice atoms as long as they are energetic enough. If the energy of the PKA is high enough, there will be a series of displacements initiated by this single PKA. Since the free path of a heavy ion is small, displacements will occur locally, and a displacement cascade ensues. In this process, the minimum energy transferable is the displacement threshold energy, E_{kd} , of the target atom, which is 92.6 eV and 16.3 eV for silicon and carbon, respectively [24]. In order to transfer this amount of energy from species i to species k , the knock-on atom of specie i must have energy no less than E_{kd}/Λ_{ik} . Below this energy, a knock-on atom of species i cannot displace an atom of species k anymore and the knock-on atom is captured.

Capture events are treated via a threshold capture energy value represented by the step function $\Gamma(E - T - E_{jd}/\Lambda_{ij})$. In the event that $i = j$ (i.e., similar species), $\Lambda_{ij} = 1$ and the minimum energy required for displacement is E_{jd} . When the species are different, the minimum energy required is E_{jd}/Λ_{ij} . This procedure is equivalent to the treatment given by Parkin and Coulter [6]. However, in our calculations, the displacement cross section is found to be insensitive to the capture events.

The PKA may collide only with electrons in dx and not cause displacement. The energy transferred to electrons, T_e , is used in electronic excitations. The PKA is left with energy $E - T_e$, which will be used in displacing lattice atoms or exciting electrons in the subsequent steps.

The PKA may collide with nothing in dx and keep its original energy E , which will then be used in displacing lattice atoms or exciting electrons in the subsequent steps.

2.5. The primary recoil spectrum

When a diatomic materials is irradiated by a neutron, PKA's may be of type i or type j . The primary recoil spectrum (PRS) depends on three factors: (1) the neutron scattering cross section with each specie, (2) the anisotropy of neutron elastic scattering cross section, and (3) the neutron spectrum. The number of

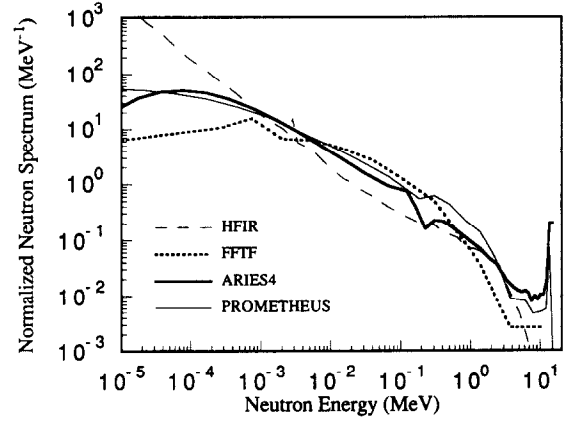


Fig. 1. Neutron spectra in several fusion and fission facilities.

PKAs of type i per unit energy at energy E is defined as

$$P_i(E) = \int_{E_{n,\min}}^{E_{n,\max}} \Phi(E_n) \sum_{1=\text{all channels}} 2\pi\sigma_{1,i}(E_n, \theta) \times \left| \frac{d \cos \theta}{dE} \right| dE_n, \quad (8)$$

where $\Phi(E_n) dE_n$ is the neutron flux from energy E_n to $E_n + dE_n$, $\sigma_{1,i}(E, \theta)$ is the differential scattering cross section of a neutron with specie i in nuclear channel 1 (e.g., elastic, (n, n') , (n, p) , (n, α) , (n, γ) nuclear reactions). The neutron spectra [15,16,17] for several facilities are shown in fig. 1. The neutron elastic cross section of silicon at low energies ($E_n \leq 2$ MeV) is given by Hughes and Schwartz [26]. Other neutron cross sections are obtained from the ENDF-V library [25]. The reasons for this choice are two fold: (1) the neutron elastic cross section of silicon at low energies is not available in ENDF-V, and (2) the neutron elastic cross section of carbon deducted from the total neutron cross section given by Hughes and Schwartz [26] is in good agreement with that obtained from ENDF-V [25]. The neutron elastic cross sections for silicon and carbon are compared in fig. 2 [25,26].

For the elastic collision channel, we have

$$E_{\min} = 0, \quad E_{\max} = \Lambda_{ni} E_n, \quad \left| \frac{d \cos \theta}{dE} \right| = \frac{2}{\Lambda_{ni} E_n}, \quad (9)$$

where Λ_{ni} is the energy transfer efficiency between a neutron and species i . For the (n, γ) nuclear reaction

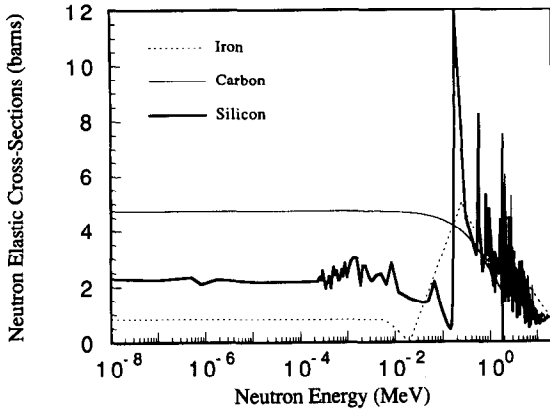


Fig. 2. Comparison of neutron elastic scattering cross sections of carbon and silicon.

channel, we find that the minimum (E_{\min}) and maximum (E_{\max}) transferred energies are given by

$$E_{\min/\max} = \frac{E_n}{1+A_i} + \frac{1}{2(1+A_i)} \left(\frac{A_i}{1+A_i} \frac{E_n}{c} - \frac{Q_{i,\gamma}}{c} \right)^2 \mp \frac{\sqrt{2E_n}}{1+A_i} \left(\frac{A_i}{1+A_i} \frac{E_n}{c} - \frac{Q_{i,\gamma}}{c} \right) \quad (10)$$

and

$$\left| \frac{d \cos \theta}{dE} \right| = \frac{1+A_i}{\sqrt{2E_n}} \left(\frac{A_i}{1+A_i} \frac{E_n}{c} - \frac{Q_{i,\gamma}}{c} \right)^{-1} \quad (11)$$

For a given (n, x) nuclear reaction channel, ($x = n', p, \alpha, \text{etc.}$), we get

$$E_{\min/\max} = \frac{B_i E_n}{(1+A_i)^2} + \left(\frac{A_i E_n}{1+A_i} - Q_{i,1} \right) \left(1 + \frac{B_i}{x} \right)^{-1} \mp \frac{2}{1+A_i} \sqrt{\left(\frac{A_i E_n^2}{1+A_i} - Q_{i,1} E_n \right) \left(\frac{1}{x} + \frac{1}{B_i} \right)^{-1}} \quad (12)$$

and

$$\left| \frac{d \cos \theta}{dE} \right| = \frac{1+A_i}{2} \sqrt{\left(\frac{1}{x} + \frac{1}{B_i} \right) \left(\frac{A_i E_n^2}{1+A_i} \right)^{-1}} \quad (13)$$

where c is the speed of light, A_i is the mass number of species i , $B_i = A_i + 1 - x$ the mass number of the resulting atom in reaction, $Q_{i,1}$ the neutron reaction energy of specie i in channel 1, $s = A_{B_j}/A_{ij}$ a scale

factor which accounts for (n, α) , (n, p) , and (n, γ) reactions.

There are several reasons for using s to account for (n, α) , (n, p) and (n, γ) channels. First, a (n, α) reaction produces a PKA that is dramatically different from the lattice atom. The associated Q -value is large, while the cross section is small. Secondly, the PKA is not too much different from the lattice atom in (n, p) and (n, γ) channels, as far as the electronic stopping power and atomic scattering cross sections are concerned. The last and the most important factor is that even for fusion neutron spectra, the neutron elastic collision channel still dominates. All other channels contribute a small fraction of the total cross section. But if neutron sources with higher neutron energies are used, non-elastic nuclear reaction channels have to be carefully studied.

In the present study, we only consider elastic, (n, n') , (n, p) , (n, α) and (n, γ) nuclear reactions channels because other channels have very higher Q -values (≤ 10 MeV), small cross sections or both, for neutrons with energy less than 15 MeV.

2.6. The displacement cross section and damage rate

We define the partial displacement cross section as

$$\sigma_{ij}(E_n) = \sum_{1=\text{all channels}} 2\pi \int_{E_{\min}}^{E_{\max}} s \sigma_{1,i}(E_n, \theta) \left| \frac{d \cos \theta}{dE} \right| \times [\nu_{ij}(E) + \delta_{ij}] dE \quad (14)$$

Because each species in a polyatomic material has different neutron cross sections, the probability that a neutron will collide with species i is $N_i \sigma_{t,i}(E_n) / \sum_j N_j \sigma_{t,j}(E_n)$. However, the probability that a PKA will collide with species i is simply assumed to be proportional to the atomic density of species i . Based on these arguments, the partial displacement cross section for lattice atom i is given by

$$\sigma_{\text{lattice } i} = f_i \sum_k \frac{N_k \sigma_{t,k}(E_n)}{\Sigma_t(E_n)} \sigma_{ki}(E_n) \quad (15)$$

where $\sigma_{t,k}(E_n)$ is the total neutron microscopic cross section of species k , $\Sigma_t(E_n)$ the total macroscopic neutron cross section of the composite.

The displacement damage rate of species i is given as

$$R_{\text{lattice } i} = \int_{E_{\min}}^{E_{\max}} \sigma_{\text{lattice } i}(E_n) \Phi(E_n) dE_n \quad (16)$$

The total displacement cross section and total displacement damage rate are simply given as the summation of the partial displacement cross sections and partial damage rates, respectively. Similarly we can define the partial displacement cross section corresponding to PKA of type i as

$$\sigma_{\text{PKA } i}(E_n) = \frac{N_i \sigma_{t,i}(E_n)}{\sum_t \sigma_t(E_n)} \sum_k f_k \sigma_{ik}(E_n). \quad (17)$$

The corresponding displacement damage rate $R_{\text{PKA } i}$ can be calculated in the same way as $R_{\text{lattice } i}$.

3. Cascade stoichiometry

It is clear from the formulation presented here that the displacement damage rates of various elements in a polyatomic solid can be vastly different. If the displacement damage rates of various elements are not in proportion to their stoichiometry in the matrix, the possibility of non-stoichiometric microstructure formation will exist. Asymmetries in displacement threshold energies for various elements in the material, different nuclear reaction cross sections, and different electronic energy losses for various elements in the material can lead to non-stoichiometric cascades. Let's now define the displacement cascade stoichiometry ratio as

$$S_{ij} = \frac{R_{\text{lattice } i}}{R_{\text{lattice } j}} - S_{\text{mat}}, \quad (18)$$

where S_{mat} is the thermodynamic stoichiometric ratio of the matrix, which is 1 for stoichiometric SiC. If S_{ij} is zero, then the cascade stoichiometry is the same as that of the matrix. Otherwise, the cascade is considered to be non-stoichiometric.

To gain insight into the type of PKA which results in more damage, we define the PKA damage ratio as

$$\text{PR}_i = \frac{R_{\text{PKA } i}}{\sum_j R_{\text{PKA } j}}. \quad (19)$$

4. Results

The electronic stopping power of carbon in carbon is shown in fig. 3, where eqs. (1)–(3) are used. The general fit given by eq. (3) gives good agreement with the experimental data reported by Northcliffe [20]. It is noted that the electronic stopping power at high PKA energies deviates substantially from the Lindhard's

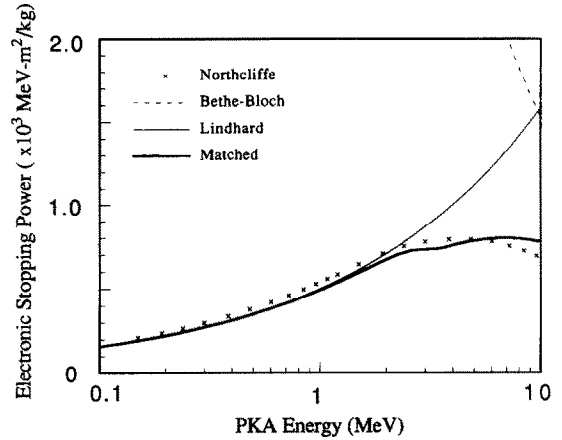


Fig. 3. Comparison of experimental and theoretical electronic stopping powers for carbon in carbon.

model. For carbon PKA with energies greater than ~ 2 MeV, the Lindhard's model would tend to overestimate the electronic energy loss. Thus for fusion neutrons, this effect is expected to play an important role. For silicon, however, the deviation from Lindhard's model at PKA energies relevant to fusion applications is small.

The primary recoil spectra for carbon and silicon based on eq. (8), under several neutron irradiation conditions, are shown in figs. 4 and 5. It is seen that the primary recoil spectrum resulting from fusion neutron irradiation and that resulting from fission neutron irradiation are very different at high PKA energies. This fact directly corresponds to the differences of the

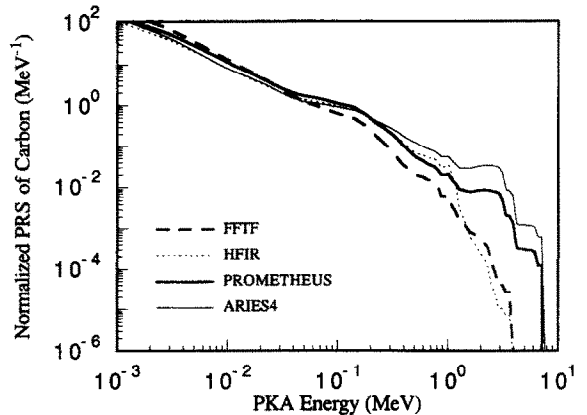


Fig. 4. Primary recoil spectra of carbon in several fusion and fission facilities.

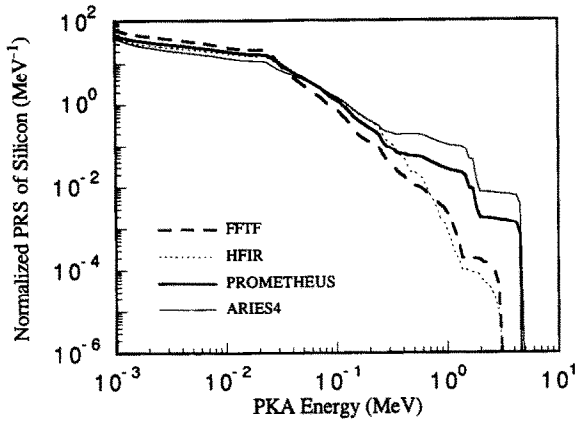


Fig. 5. Primary recoil spectra of silicon in several fusion and fission facilities.

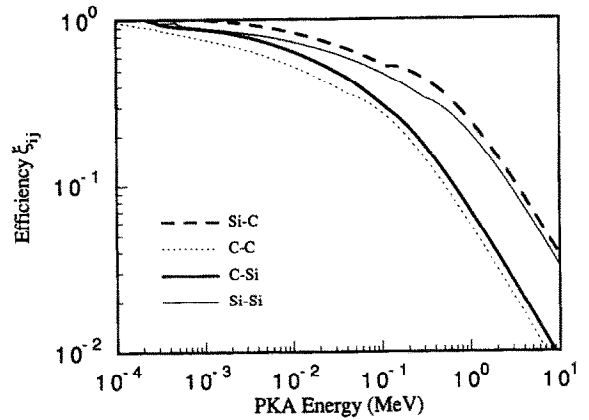


Fig. 6. Displacement efficiency ξ_{ij} . The first subscript is PKA while the second is the lattice atom being displaced.

neutron spectra shown in fig. 1. The result may have important implications for the simulation of fusion neutron damage with fission neutrons.

The fraction of energy which is dissipated in atomic displacements rather than heat is defined as the damage efficiency. This fraction is shown in fig. 6, where we show ξ_{ij} as the fraction of energy used in displacements in the process that ion i displaces lattice atoms j . It is seen that the damage efficiency for carbon is lower than that for silicon, particularly at higher energies, because of the higher electronic stopping power of C in SiC. At high energies, although the electronic energy loss decreases as a function of energy, the scattering cross section decreases at a faster rate, with the net effect being a decrease in the displacement efficiency. This is exemplified for carbon ions at high PKA energies in fig. 6. There are two factors which determine the number of displaced atoms by a given transferred energy: (1) the electronic stopping power, and (2) the displacement threshold. Fig. 7 demonstrates the energy dependence of the number of displaced atoms, ν_{ij} , obtained by solving the coupled integro-differential equations.

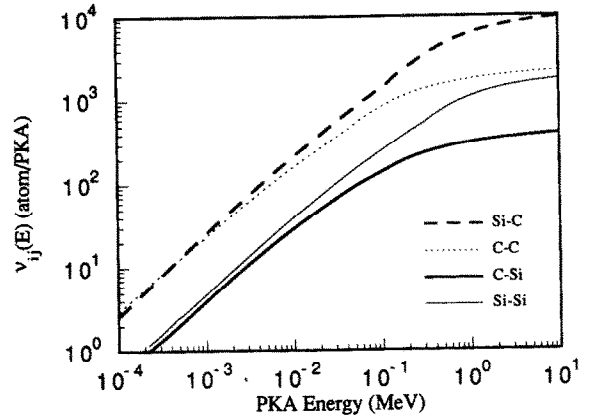


Fig. 7. Number of displaced atoms of type j caused by PKA of type i , ν_{ij} .

The partial displacement cross sections defined in eq. (14) and the total displacement cross section are shown in fig. 8. The important fact to mention here is that the displacement cross section of SiC is very different from that of steel, as calculated by Doran [3]. If the neutron spectrum is composed mainly of fast neutrons ($0.1 \text{ MeV} \leq E_n \leq 1 \text{ MeV}$), the displacement damage rate of SiC will be larger than that of steel. On the other hand, if the neutron spectrum is composed mainly of fusion neutrons, the damage rate of SiC will

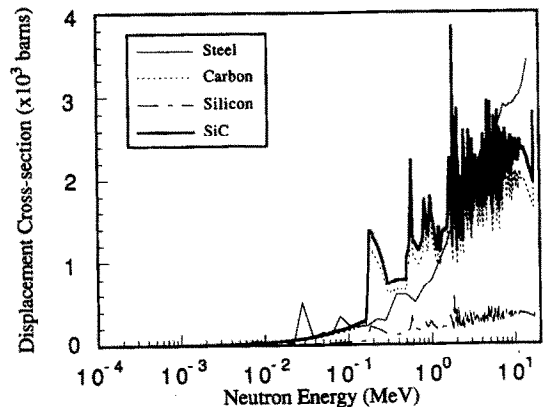


Fig. 8. Displacement cross sections for SiC. Also shown is the displacement cross section for steel calculated by Doran [3].

Table 1
Displacement damage rates (dpa) and cascade stoichiometry for SiC

Species	Facility				
	ARETS-4 [17]	PROMETHEUS [16]	FFTF [15]	HFIR [15]	NRU [15]
Carbon	11.5	13.7	62.5	32.7	21.4
Silicon	2.1	2.5	11.2	5.8	3.8
Total	13.6	16.2	73.7	38.5	25.2
S_{C-Si}	4.5	4.5	4.6	4.6	4.6
PR_c	0.27	0.33	0.35	0.34	0.34
Location	First wall	First wall	Midplane in MOTA	Instrumented position	Markiv fast neutron rod
Normalization	MW-y/m ²	MW-y/m ²	10 ²⁷ n/m ²	10 ²⁷ n/m ²	10 ²⁷ n/m ²

be smaller than that of steel. The reasons for these can be seen by referring to fig. 2. The nuclear elastic cross section of Si or C is higher than that of iron in the neutron energy range (0.1 MeV–1 MeV), and lower than that of iron for fusion neutrons.

Based on eq. (15), the partial displacement damage rate of silicon and carbon, the total displacement damage rate and the two fractions defined in section 3 are calculated for typical fusion reactors, a fast fission reactor, a mixed spectrum reactor and a thermal fission reactor. The calculated results are listed in table 1. From the table, one can see that thermal neutrons do not result in significant displacement damage in SiC. The displacement damage rate for a typical fusion reactors is on the order of ~ 15 dpa/year for 1 MW/m² neutron wall loading.

5. Conclusions

The results of our calculations reveal many features of the displacement damage process for SiC in a neutron environment. Salient conclusions are given below.

(1) The total displacement cross section of SiC for epithermal neutrons is small. However, the displacement cross section for fast neutrons ($0.1 \text{ MeV} \leq E_n \leq 1 \text{ MeV}$) is larger than that of steel. The damage rate is also smaller than that of steel for fusion neutrons. This may have important implications for the simulation of fusion neutron damage with fission neutrons. Therefore, fast reactor irradiation will accelerate damage production in comparison to fusion reactors.

(2) The local stoichiometry of SiC will be dramatically changed after irradiation, because carbon atoms are easily displaced due to their small displacement threshold. Approximately 80% of the displaced atoms will be carbon-type. It is experimentally found [27] that

SiC does not amorphize if the irradiation temperature is above 650°C. The thermo-chemical driving forces for recrystallization are strong enough to restore the best stoichiometry.

(3) The displacement damage rate for typical magnetic confinement fusion conditions is around 14 dpa/year for 1 MW/m² neutron wall loading, that for typical inertial confinement fusion conditions is around 16 dpa/year for 1 MW/m² neutron wall loading, that for FFTF is around 74 dpa per 10²⁷ n/m², that for HFIR is around 39 dpa per 10²⁷ n/m², and that for NRU is around 25 dpa per 10²⁷ n/m². The damage rate is sensitive to the neutron spectrum, i.e. the design.

(4) The interpretation of simulation experiments with energetic particles (up to 100 MeV) requires further analysis. Non-elastic neutron scattering channels will become important in this case. Subsequently, the number of PKA species will be larger than the number of lattice species.

Appendix A. Extension of the Runge–Kutta method

Assume that we have the following coupled differential equations:

$$dy/dx = f(x, y, z), \quad (\text{A.1})$$

$$dz/dx = g(x, y, z). \quad (\text{A.2})$$

Now let

$$K_1 = f(x_i, y_i, z_i), \quad (\text{A.3})$$

$$M_1 = g(x_i, y_i, z_i), \quad (\text{A.4})$$

$$K_2 = f(x_i + p_1 h, y_i + q_1 K_1 h, z_i + r_1 M_1 h), \quad (\text{A.5})$$

$$M_2 = g(x_i + p_2 h, y_i + q_2 K_1 h, z_i + r_2 M_1 h), \quad (\text{A.6})$$

where h is the increment of the independent variable, y_i and z_i are the solutions for y and z at point x_i , p_1 , q_1 , r_1 , p_2 , q_2 , and r_2 are free parameters. The goal is to approximate y_{i+1} and z_{i+1} to h^3 by choosing the free parameters

$$y_{i+1} = y_i + (a_1 K_1 + a_2 K_2)h, \quad (\text{A.7})$$

$$z_{i+1} = z_i + (b_1 M_1 + b_2 M_2)h, \quad (\text{A.8})$$

where a_1 , a_2 , b_1 and b_2 are also free parameters.

On the other hand, the Taylor expansion of y_{i+1} can be written as

$$y_{i+1} = y_i + f(x_i, y_i, z_i)h + \frac{1}{2} \frac{df}{dx}(x_i, y_i, z_i)h^2 + O(h^3), \quad (\text{A.9})$$

while

$$\frac{df}{dx} = \frac{\partial f}{\partial x} + \frac{\partial f}{\partial y} \frac{dy}{dx} + \frac{\partial f}{\partial z} \frac{dz}{dx}. \quad (\text{A.10})$$

K_2 and M_2 can also be expanded in Taylor series as

$$K_2 = f(x_i, y_i, z_i) + p_1 h \frac{\partial f}{\partial x} + q_1 K_1 h \frac{\partial f}{\partial y} + r_1 M_1 h \frac{\partial f}{\partial z}, \quad (\text{A.11})$$

$$M_2 = g(x_i, y_i, z_i) + p_2 h \frac{\partial g}{\partial x} + q_2 K_1 h \frac{\partial g}{\partial y} + r_2 M_1 h \frac{\partial g}{\partial z}. \quad (\text{A.12})$$

Substituting K_1 and K_2 into expression of y_{i+1} and comparing the coefficients of independent functions, we obtain

$$a_1 + a_2 = 1 \oplus a_2 p_1 = \frac{1}{2} \oplus a_2 q_1 = \frac{1}{2} \oplus a_2 r_1 = \frac{1}{2}. \quad (\text{A.13})$$

There are four equations and 5 unknowns, so we can choose

$$p_1 = 1 \oplus q_1 = 1 \oplus r_1 = 1 \oplus a_1 = \frac{1}{2} \oplus a_2 = \frac{1}{2}. \quad (\text{A.14})$$

Similarly, we can find the free parameters in expression for z_{i+1} . Therefore,

$$y_{i+1} = y_i + \frac{1}{2} h (K_1 + K_2), \quad (\text{A.15})$$

$$z_{i+1} = z_i + \frac{1}{2} h (M_1 + M_2). \quad (\text{A.16})$$

Using this method, we have a numerical calculation which is accurate up to h^3 . For our problem, $h = E_i(e^{c/n} - 1)$ with $c = \log(E_{\max}/E_{\min})$, n the chosen number for discretizing the energy range, E_i as the PKA energy at i th discretized energy point. Because of electronic stopping, $\nu_i \propto E^\alpha$ with $\alpha < 1$. Therefore, the relative error at any step is less than $(e^{c/n} - 1)$.

Appendix B. Nuclear reaction kinematics

In the following, we derive the kinematics for (n, γ) and other non-elastic nuclear reaction channels. For (n, γ) reactions, the conservation of momentum and that of energy give

$$E/c = (1+A)u_{2f}, \quad (\text{B.1})$$

$$E + \frac{1}{2}(1+A)u_{2f}^2 + Q = \frac{1}{2}u_{1o}^2 + \frac{1}{2}Au_{2o}^2, \quad (\text{B.2})$$

where E is the emitted γ -ray energy. A the mass number of target atom, Q the nuclear reaction energy of the (n, γ) reaction, u the speed of particle in CMS, the subscript 1 and 2 are for neutron and target atom respectively, the subscript o and f are for before and after reaction, respectively, and c the speed of light. The energy and momentum are in atomic units. Solving these two equations for non-relativistic condition, we have

$$u_{2f} = \frac{AE_n}{c(1+A)^2} - \frac{1}{(1+A)} \frac{Q}{c}. \quad (\text{B.3})$$

Assuming that the scattering angle in CMS is θ , we have the velocity of the resulting atom in LS

$$V_{2f} = \left(\frac{V_{1o}^2}{(1+A)^2} + \left[\frac{AE_n}{c(1+A)^2} - \frac{1}{1+A} \frac{Q}{c} \right]^2 - \frac{2V_{1o}}{1+A} \left[\frac{AE_n}{c(1+A)^2} - \frac{1}{1+A} \frac{Q}{c} \right] \cos \theta \right)^{1/2}, \quad (\text{B.4})$$

where V_{1o} is the speed of incident neutron in LS. The kinetic energy of the resulting atom (i.e., the energy transferred to target atom) is given by

$$E = \frac{E_n}{1+A} + \frac{1}{2(1+A)} \left(\frac{A}{1+A} \frac{E_n}{c} - \frac{Q}{c} \right)^2 - \frac{\sqrt{2E_n}}{1+A} \left(\frac{A}{1+A} \frac{E_n}{c} - \frac{Q}{c} \right) \cos \theta. \quad (\text{B.5})$$

For (n, x) reactions ($x = n', p, \alpha, 2n$, etc.), the conservation of momentum and that of energy give

$$xu_{1f} = Bu_{2f} \quad (\text{B.6})$$

$$\frac{1}{2}xu_{1f}^2 + \frac{1}{2}Bu_{2f}^2 + Q = \frac{1}{2}u_{1o}^2 + \frac{1}{2}Au_{2o}^2, \quad (\text{B.7})$$

where x is the mass number of emitted particle (e.g., $n', p, \alpha, 2n$, etc.), B the mass number of resulting atom. Other notations are the same as those used in

(n, γ) reaction. Solving these two equations, we have the final velocity of resulting atom in CMS,

$$u_{2f} = \sqrt{\left(\frac{2AE_n}{1+A} - 2Q\right)\left(\frac{B^2}{x} + B\right)^{-1}} \quad (\text{B.8})$$

The corresponding velocity in LS is given by

$$V_{2f} = \left(\frac{2E_n}{(1+A)^2} + \left[\frac{2AE_n}{1+A} - 2Q\right]\left[\frac{B^2}{x} + B\right]^{-1} - \frac{4 \cos \theta}{1+A} \sqrt{\left[\frac{AE_n^2}{1+A} - QE_n\right]\left[\frac{B^2}{x} + B\right]^{-1}}\right)^{1/2} \quad (\text{B.9})$$

The energy transferred to the target atom is therefore

$$E = \frac{BE_n}{(1+A)^2} + \left[\frac{AE_n}{1+A} - Q\right]\left[\frac{B}{x} + 1\right]^{-1} - \frac{2 \cos \theta}{1+A} \sqrt{\left[\frac{AE_n^2}{1+A} - QE_n\right]\left[\frac{1}{x} + \frac{1}{B}\right]^{-1}} \quad (\text{B.10})$$

Acknowledgements

The authors would like to thank Dr. M. Youssef at UCLA and Dr. L. El-Gubaly at the University of Wisconsin for providing the neutron spectra for PROMETHEUS and ARIES-IV, respectively. Support of the US Department of Energy, Office of Fusion Energy, under grant number DE-FG03-91ER54115 is gratefully acknowledged.

References

- [1] J. Jenkins, Nucl. Sci. Eng. 41 (1970) 155.
- [2] W. Sheely, Nucl. Sci. Eng. 29 (1967) 165.
- [3] D. Doran, Nucl. Sci. Eng. 49 (1972) 130.
- [4] E. Baroody, Phys. Rev. 112 (1958) 1571.
- [5] N. Andersen and P. Sigmund, Mat. Fys. Medd. 39 (1974) 3.
- [6] D. Parkin and C. Coulter, J. Nucl. Mater. 85 & 86 (1979) 611.
- [7] L. Greenwood, Reactor Dosimetry: Methods, Applications and Standardization, ASTM-STP 1001, eds. H. Ferrar IV and E. Lippincott (American Society for Testing and Materials, Philadelphia, 1989) pp. 598–602.
- [8] A. Alberman and D. Lesueur, *ibid.* ref. [7], pp. 576–591.
- [9] J. Lindhard and M. Scharff, Mat. Fys. Medd. 27 (1953) 15.
- [10] J. Lindhard and M. Scharff, Phys. Rev. 124 (1961) 128.
- [11] H. Bethe, Ann. Physik 5 (1930) 325.
- [12] F. Bloch, Ann. Physik 16 (1933) 285.
- [13] J. Biersack and L. Haggmark, Nucl. Instr. and Meth. 174 (1980) 257.
- [14] N. Ghoniem, Validity of Bragg's Stopping Cross Section Additivity Rule for SiC, Master's Thesis, McMaster University, May 1974.
- [15] M. Abdou et al., Modeling, Analysis and experiments for Fusion Nuclear Technology, PPG-1021, UCLA-ENG-86-44, FNT-17 (1987) chap. 2.
- [16] Personal communications with Dr. M. Youssef at UCLA about PROMETHEUS.
- [17] Personal communications with Dr. L. El-Gubaly at University of Wisconsin about ARIES-IV.
- [18] J. Ziegler, J. Biersack and U. Littmark, The Stopping and Range of Ions in Solids, chap. 3 (Pergamon, London, 1985).
- [19] N. Bohr, Phys. Rev. 59 (1941) 270.
- [20] L. Northcliffe and R. Schilling, Nucl. Data Tables A7 (1970) 233.
- [21] K. Winterbon, P. Sigmund and J. Sanders, Mat. Fys. Medd. 37 (1070) 14.
- [22] P. Chou, A Monte Carlo Approach to Ion Transport in Solids and Its Applications to Bulk and Surface Damage Analysis, Ph.D. Thesis at UCLA, May 1986.
- [23] K. Atkinson, An Introduction to Numerical Analysis, 2nd ed. (John Wiley, New York, 1988) chap. 7.
- [24] A. El-Azab and N. Ghoniem, J. Nucl. Mater. 191–194 (1992) 1110.
- [25] ENDF-V, JENDL-3, evaluated by JAERI and TIT, updated on December 19, 1991.
- [26] D. Hughes and R. Schwartz, Neutron Cross Sections (US Government Printing Office, Washington, DC, 1958).
- [27] K. Okamura, T. Matsuzawa, M. Sato, H. Kayano, S. Morozumi, H. Tezuka and A. Kohyama, J. Nucl. Mater. 155–157 (1988) 329.